

**Magnetoelectric Bistability of Molecular Ferroic Solids**

Journal:	<i>Journal of Materials Chemistry C</i>
Manuscript ID	TC-COM-05-2019-002641.R1
Article Type:	Communication
Date Submitted by the Author:	01-Jul-2019
Complete List of Authors:	Guan, Yingshi; University at Buffalo - The State University of New York, Hu, Yong ; University at Buffalo - The State University of New York Li, Changning; University at Buffalo - The State University of New York, School of Engineering and Applied Sciences Ren, Shenqiang; University at Buffalo - The State University of New York,



Magnetoelectric Bistability of Molecular Ferroic Solids

Ying-Shi Guan,[#] Yong Hu,[#] Changning Li, and Shenqiang Ren*

Received 00th January
20xx,
Accepted 00th January
20xx

DOI: 10.1039/x0xx00000x

www.rsc.org/

Organic multiferroics showing electrical and magnetic bistability on molecular scale is essential as the foundation for the miniaturized logic gates and memories. However, low Curie temperature in organic multiferroics limited its practical applications in molecular electronics. Here we suggest a different magnetoelectric coupling approach through organic multiferroic composite. We show that molecular ferroic solids exhibit the switchable electrical, dipole and magnetic bistability around room temperature. The switchable magnetoelectricity is shown under laser shock impact, as well as an anomalies magnetization around ferroelectric Curie temperature. The coupling between charge, dipole and spin order parameters enables a demonstration of tailoring magnetoelectricity and conductivity in molecular ferroic solids.

1 Introduction

Information processing and switching rely on the ability to retrieve and control changes in a particular physical property of a material, such as the electrical, thermal, magnetic, or optical response. In this context, one of these physical channels can be usually utilized at the level of the basic unit. When two or more different physical channels of the material are simultaneously involved, a new breadth of applications and even new fields of research often appear, such as optoelectronics, multiferroics, and quantum dipole liquid.¹⁻³ Among them, an enormous attention has been drawn in magnetoelectric multiferroics, where magnetic and electric orders coexist, providing an efficient way for the mutual control of magnetism and ferroelectricity in functional materials.⁴⁻¹⁰ The coupling of ferroic orders allows the tuning of two or more physical parameters under external stimuli to generate novel functionalities which do not exist in either single state.^{6, 11-13} Stimuli controlled ferroic coupling in multiferroics suggests its emerging applications, such as memories, sensors, and spin-nanoelectronics.^{8, 9} However, single-phase organic multiferroics are relatively rare which raises the fundamental interest in discovering the coexistence of ferroic orders.¹⁴⁻¹⁶

Previous study on multiferroic materials has been mostly focused on inorganic compounds and composites materials, organic multiferroics materials have been studied rarely. Up to now, only few examples of coexisting electric and magnetic orders within organic materials have been reported in multiferroics, like metal-organic frameworks,^{4, 15, 17} and organic charge-transfer salts.⁷ In addition, the common challenge of low Curie temperature in organic multiferroics limited its practical applications in molecular electronics.^{7, 8} Very recently enormous attention has been drawn in polycyclic aromatic hydrocarbons (PAHs)

due to the recent report on superconductivity in alkali, alkaline-earth metals, and rare-earth elements-doped polycyclic aromatic hydrocarbons superconductors.

Here we suggest a different magnetoelectric coupling approach through organic multiferroic composite, in which the magnetic phase is radical biphenyl ($C_{12}H_{10}^{\cdot}$) obtained from alkali-metal-intercalated biphenyl.¹⁸⁻²⁰ By reacting with potassium, the radical biphenyl ($C_{12}H_{10}^{\cdot}$) shows the spin ordering and tunable magnetism at different doping levels. The low ratio between potassium and biphenyl can form antiferromagnetic ground state.¹⁹ Organic ferroelectric phase is poly[(vinylidene fluoride-co-trifluoroethylene) (P(VDF-TrFE))], which exhibit remarkable dielectric and ferroelectric properties, together with their excellent stability to chemicals, mechanical flexibility and biocompatibility.²¹⁻²⁴ Here we study the coupling between ferroelectric and magnetic order in potassium doped biphenyl (KB) and P(VDF-TrFE) composite (KB-PT).

2 Experimental Section

2.1 Materials and instruments.

Potassium, biphenyl, PVDF-TrFE were purchased from Sigma-Aldrich and used as received. The SEM images were taken from FEI Quanta450FEG. UV-Vis spectrum was recorded on an Agilent Model HP8453 UV-vis spectrophotometer using the ground powder samples. Raman spectra were recorded on Renishaw inVia raman microscope. Magnetization curves are measured by a vibrating sample magnetometer (VSM) of Microsense and a Physical Property Measurement System with an AC measurement system option of Quantum Design. Keithley 2400 SourceMeter was used to obtain current versus voltage curves. Current probes and voltage probes contact to samples parallel and width and length between probes were about 5 mm and height of sample was about 3 mm. EPR spectra were collected using a Bruker EMX EPR spectrometer.

2.2 The synthesis of the KB samples.

Department of Mechanical and Aerospace Engineering, RENEW Institute
University at Buffalo, The State University of New York
Buffalo, NY 14260, USA

Y.-S. Guan and Y. Hu contribute equally to this work.

E-mail: shenren@buffalo.edu

*Electronic Supplementary Information (ESI) available: Optical microscopy images, SEM images and photoresponse behavior data are included in the supporting information. See DOI: 10.1039/x0xx00000x

Potassium doped biphenyl was synthesized by solid state reaction. Pure potassium lumps with small pieces and biphenyl powder with a molar ratio 1:1 were sealed in glass tubes. Glass tubes were evacuated by a turbo molecular pump and sealed under high vacuum condition. The evacuated glass tube was sintered at 180 °C for 48 hours.

2.3 The preparation of PVDF-TrFE tablet.

The preparation of PVDF-TrFE tablet is done by grinding the source materials and pressing them into a pellet (0.25 inch in diameter) at a pressure of one ton in a glove box.

2.4 The preparation of KB-PT samples.

The KB and PVDF-TrFE sample with different volume ratios were prepared by grinding the source materials and pressing them into a pellet (0.25 inch in diameter) at a pressure of one ton in a glove box. KB-PT (KB:PT=1:1; KB₁:PT₃=1:3; KB₃:PT₁=3:1).

3 Results and Discussion

Figure 1a shows the chemical structure of P(VDF-TrFE) and KB radical. The scanning electron microscopy (SEM) of KB-PT composite shows the closely packed morphology with uniform distribution of P(VDF-TrFE) and K-biphenyl (Figure 1b). The energy dispersive X-ray spectroscopy (EDS) mapping (Figure 1c) reveals the homogenous and uniform phase distribution between P(VDF-TrFE) and KB domains. The photoabsorption of KB-PT is attributed to the radical (587 and 940 nm) and diradical (640 nm) in KB (Figure S1).²⁸ Raman spectrum of KB at 1,245 and 450 cm⁻¹ indicates the significant contribution from the modes of the terminal rings, signaling the formation of the radicals and diradicals (Figure S2). When compared to the Raman spectrum of pure biphenyl, the KB spectrum exhibits obvious changes, the peaks at 1,590 and 1,608 cm⁻¹ in pure biphenyl coupling together centred at 1594 cm⁻¹ in KB.²⁰ The electron paramagnetic resonance (EPR) spectroscopy further confirms the existence of radicals in KB at room temperature (Figure S3), showing an isotropic signal centered at $g = 2.0029$ with a classic Lorentzian shape. The ferroelectricity of PVDF-TrFE is demonstrated by the polarization-electric field hysteresis loop (Figure S4), which shows a saturated polarization of 2.21 $\mu\text{C}/\text{cm}^2$ under the electric field of 110 kV/cm. Bistability is achieved through the switchable electric polarization in P(VDF-TrFE) domain, which controls the conductivity and dipole formation in KB. We show that electronic correlation plays a decisive role in the coupling of radical, magnetic and charge orders. A magnetoelectric coupling effect is driven by charge ordering, which can be switched by the control of external stimuli, serving as an effective way for the mutual control of radical magnetism and electric dipoles.^{12, 13}

Our recent work demonstrated that one-dimensional dipole pairs, induced by dipole interaction, regulate the conductivity, as well as the electronic, magnetic and optical transitions, in alkali-metal-intercalated aromatic molecules.²⁵ Thus, in KB-PT, ferroelectricity of P(VDF-TrFE) could largely controls the dipole formation and conductivity tuning in K-biphenyl domains through the bistability before and after electric poling, enabling a mutual control of charge and dipole moments. The mutual control of conductivity and dipole is

demonstrated by electrically switchable resistance in KB-PT, using the electric poling of P(VDF-TrFE) domains. As shown in Figure 1d, the temperature dependent resistance of KB-PT shows a typical conducting behavior originated from KB before poling. After electric polarization, the temperature dependent resistance of KB-PT exhibits a pronounced metal-insulator transition (MIT) at 250 K, with a sharp transition between two different conducting states. At a relatively high temperature range (270 K - 300 K), polaron is the dominant charge carrier accounting for the high conductivity, while decreasing the temperature together with the poling, P(VDF-TrFE) phase accumulates a large number of aligned dipoles at the interface between P(VDF-TrFE) and KB (the inset of Figure 1d). The generated dipoles induce polarons to form bipolarons in KB domains, leading to a lower mobility. Therefore, the resistance of KB-PT have a sharp increase at the transition temperature, with an order of magnitude increase from 250 K to 270 K (Figure 1d). Temperature dependent magnetization (M-T) of KB simultaneously shows a transition at 250 K from paramagnetism to diamagnetism, confirming the polaron to singlet bipolaron transition (Figure S5).

The correlation between charge, dipole, and spin orders is further demonstrated through temperature dependence of relative permittivity. As shown in Figure 1e, temperature dependent relative permittivity of KB-PT shows a pronounced peak, reaching the absolute value up to 37 at ~250 K. In addition, the dielectric amplitude of KB-PT becomes strongly suppressed as increasing the frequency. The polarization-induced dipoles in P(VDF-TrFE) phase accumulate at the phase boundary and facilitate electric dipole formation within the KB phase, leading to the pronounced relative permittivity of KB at 250 K within a low frequency range. While at a high frequency, the slow response of electric dipoles leads to the diminished relative permittivity. The charge-spin interactions in KB can induce the magnetic field effect on dielectric response. As increasing magnetic field, temperature dependent relative permittivity of KB-PT become suppressed (Figure 1f), suggesting the origin of electric dipoles within the KB domains. Meanwhile, it should be noted that no dielectric transition is observed within the pristine P(VDF-TrFE) and KB. This confirms the polarization effect of P(VDF-TrFE) on electric dipoles in KB, leading to the bistability of KB-PT.

The resistance modulation in KB-PT is further illustrated in Figure 2a, where electrically switchable resistance of KB-PT is controlled by electric poling field. The ferroelectric domain provides the driving force of the resistance switching. Without electric poling, the polarization and dipoles in P(VDF-TrFE) phase are randomly distributed. The charge transport in KB-PT is dominant by intrinsic charge transport from the KB phase. The KB exhibits a semiconducting behavior (Figure S6). When an electric poling field is applied between two opposite directions, the upward and downward polarization facilitates or hinders the charge transport in the KB phase, respectively. A relative small electric field (reading electric field) is applied to measure the resistance without changing the polarization. The low resistance state (On state) is induced when the polarization direction is parallel to the reading electric field direction due to the decreased potential barrier. However, the resistance will go up when KB-PT is polarized in the opposite direction of reading electric field, resulting in a high resistance state (Off state) due to the increased

potential barrier (Figure 2a). The current-voltage (I-V) curves for the "On" and "Off" states is shown in Figure 2b, which exhibits significant difference in resistance between two states. Retention performance (inset of the Figure 2b) is also studied for On and Off states in KB-PT. It is clearly shown that On and Off state are stable over 2 hours. A slight change in resistance are shown in Figure 2c during the continuous measurement under the On and Off state also indicates its good retention performance. The reproducibility of the switching performance in KB-PT is further measured by repeatedly switching the ferroelectric barrier with positive and reverse poling. As shown in Figure 2d, the On/Off resistance ratio of about 40 can be repeated more than 50 cycles. These results demonstrate that the polarization switching controls high resistance (Off) state and low resistance (On) state in KB-PT with remarkable retention and recyclability, through modulating the potential barrier height.

High strain-rate laser shock processing (10^5 - 10^6 S⁻¹) is a new and efficient way to study non-equilibrium ferroic coupling in KB-PT. The P(VDF-TrFE) exhibits remarkable electromechanical coupling, while the applied external pressure leads to free charges on the surface of P(VDF-TrFE). Figure 3a illustrates the pressure generated by laser shock wave effect on P(VDF-TrFE) phase, so that the charge transport at the interface between P(VDF-TrFE) and KB can be effectively modulated. According to Fabbro's model,^{26, 27} the pressure of the shock wave generated by the laser pulse can reach 0.85 to 1.83 GPa depending on the applied intensity and pulse duration. As shown in Figure 3b, the resistance of the interface is decreased dramatically under a laser shock wave. The interface resistance is decreased by 8.5%, 13%, and 26% with external pressure of 0.75 GPa, 0.88 GPa, and 1.0 GPa, respectively. High pressure impact on the P(VDF-TrFE), due to the piezoresponse, can generate a large density of free charge carriers to facilitate the charge transport in KB. The pressure-dependent magnetization is further carried out in KB-PT (Figure 3c). The enhanced magnetization under pressure suggests the coupling of magnetic and electric order parameters in KB-PT, where the piezoelectrically induced charge ordering by uniaxial compression lead to the polaron formation of KB, which in turn enhance the spin order.

To further demonstrate the mutual control of magnetism and electricity, we carry out the temperature-dependent magnetization (M-T) in KB-PT. As shown in Figure 4a, the magnetization of KB-PT exhibits a pronounced enhancement of 28% at the ferroelectric transition temperature (~ 373 K) of P(VDF-TrFE).^{21,22} The pronounced dielectric peak of P(VDF-TrFE) phase suggests the ordering of electric dipoles below the order-disorder transition temperature, while the accumulated charge orders lead to the increase of the magnetization of KB, as observed in M-T curve. In addition, The M-T (Figure S7) measurements of KB₁-PT₃ and KB₃-PT₁ shows that the ratio of KB and P(VDF-TrFE) plays an important role in the magnetoelectric coupling effect, where a low or high KB ratio does not show pronounced change in the magnetization at the ferroelectric transition temperature. Furthermore, tuning and controlling magnetization of KB-PT is carried out by applying electric field as a function of time (The inset of Figure 4b). When an external electric field is applied, the aligned dipoles in the P(VDF-TrFE) phase induce the formation of polarons in KB phase, which in turn affects the spin

ordering and polarization. Therefore, a tunable magnetization of KB-PT can be observed under different external electric fields (Figure 4b). To further demonstrate the magnetoelectric coupling of the spin and dipole order, we demonstrate that the electric field dependence of converse ME coupling coefficient (α) can range from 2.93 ps/m to 3.14 ps/m under different external magnetic fields (Figure 4c), where the optimum α is achieved at 100 Oe external bias magnetic field and electrical field of 200 V/cm.

Conclusion

In summary, we show that molecular ferroic solids, composed of ferroelectric molecular radical solid, exhibit the electrical, dipole and magnetic bistability for switching around transition temperature. The non-equilibrium laser shock impact facilitates the switchable conductivity and bistability in KB-PT through the piezoelectric effect. We demonstrate that spin and charge orders are strongly coupled in organic multiferroic material. The couplings between spin and charge orders are manifested as a mutual control of dipole, conductivity and magnetoelectricity. Both temperature-dependence and voltage-controlled magnetization signal the magnetoelectric coupling through a change of magnetization of KB-PT at ferroelectric Curie temperature. This work highlights the promise of the organic magnetoelectric materials through the coupling between ferroelectric domain and radical hydrocarbon domain.

Acknowledgements

Y.-S. Guan and Y. Hu contribute equally to this work.

The U.S. Department of Energy, Office of Basic Energy Sciences, Division of Materials Sciences and Engineering supports S.R. under Award DE-SC0018631 (Organic conductors). Financial support was provided by the U.S. Army Research Office supports S. R. under Award W911NF-18-2-0202 (Materials-by-Design and Molecular Assembly)

Notes and references

1. H. Gibbs, *Optical bistability: controlling light with light*, Elsevier, 2012.
2. M. Itkis, X. Chi, A. Cordes and R. Haddon, *Science*, 2002, **296**, 1443-1445.
3. N. Hassan, S. Cunningham, M. Mourigal, E. I. Zhilyaeva, S. A. Torunova, R. N. Lyubovskaya, J. A. Schlueter and N. Drichko, *Science*, 2018, **360**, 1101-1104.
4. D. W. Fu, W. Zhang, H. L. Cai, Y. Zhang, J. Z. Ge, R. G. Xiong, S. D. Huang and T. Nakamura, *Angew. Chem. Int. Ed.*, 2011, **50**, 11947-11951.
5. Z. Tu, M. Wu and X. C. Zeng, *J. Phys. Chem. Lett.*, 2017, **8**, 1973-1978.
6. F. Matsukura, Y. Tokura and H. Ohno, *Nat. Nano.*, 2015, **10**, 209.

7. P. Lunkenheimer, J. Müller, S. Krohns, F. Schrettle, A. Loidl, B. Hartmann, R. Rommel, M. De Souza, C. Hotta and J. A. Schlueter, *Nat. Mater.*, 2012, **11**, 755.
8. W. Eerenstein, N. Mathur and J. F. Scott, *Nature*, 2006, **442**, 759.
9. M. Fiebig, T. Lottermoser, D. Meier and M. Trassin, *Nat. Rev. Mater.*, 2016, **1**, 16046.
10. H. Zheng, J. Wang, S. Lofland, Z. Ma, L. Mohaddes-Ardabili, T. Zhao, L. Salamanca-Riba, S. Shinde, S. Ogale and F. Bai, *Science*, 2004, **303**, 661-663.
11. D. Khomskii, *Physics*, 2009, **2**, 20.
12. J. Van Den Brink and D. I. Khomskii, *J. Phys.: Condens. Matter*, 2008, **20**, 434217.
13. F. Schrettle, S. Krohns, P. Lunkenheimer, V. Brabers and A. Loidl, *Phys. Rev. B*, 2011, **83**, 195109.
14. Y. Zhou, D. Maurya, Y. Yan, G. Srinivasan, E. Quandt and S. Priya, *Energy Harvesting and Systems*, 2016, **3**, 1-42.
15. G.-C. Xu, W. Zhang, X.-M. Ma, Y.-H. Chen, L. Zhang, H.-L. Cai, Z.-M. Wang, R.-G. Xiong and S. Gao, *J. Am. Chem. Soc.*, 2011, **133**, 14948-14951.
16. A. Rajca, J. Wongsriratanakul and S. Rajca, *Science*, 2001, **294**, 1503-1505.
17. Y. Tian, A. Stroppa, Y. Chai, L. Yan, S. Wang, P. Barone, S. Picozzi and Y. Sun, *Sci. Rep.*, 2014, **4**, 6062.
18. W. Liu, H. Lin, R. Kang, X. Zhu, Y. Zhang, S. Zheng and H.-H. Wen, *Phys. Rev. B*, 2017, **96**, 224501.
19. G.-H. Zhong, X.-H. Wang, R.-S. Wang, J.-X. Han, C. Zhang, X.-J. Chen and H.-Q. Lin, *J. Phys. Chem. C*, 2018, **122**, 3801-3808.
20. Y. -S. Guan, Y. Hu, Y. Huang, A. F. Cannella, C. Li, J. N. Armstrong, and S. Ren. *ACS Appl. Nano Mater.* 2019, **2**, 1140-1145
21. C. Chen, P. Hu, J. Yang and Z. Liu, *Materials Science-Poland*, 2016, **34**, 650-654.
22. L. Huang, C. Lu, F. Wang and L. Wang, *RSC Advances*, 2014, **4**, 45220-45229.
23. S. El-Sayed, T. A. Abdel-Baset and A. Hassen, *AIP Adv.*, 2014, **4**, 037114.
24. J. Fu, Y. Hou, M. Zheng, Q. Wei, M. Zhu and H. Yan, *ACS Appl. Mater. Interfaces*, 2015, **7**, 24480-24491.
25. Y. Hu, G. Zhong, Y. S. Guan, N. H. Lee, Y. Zhang, Y. Li, T. Mitchell, J. N. Armstrong, J. Benedict and S. W. Hla, *Adv. Mater.*, 2019, 1807178.
26. H. Gao, Y. Hu, Y. Xuan, J. Li, Y. Yang, R. V. Martinez, C. Li, J. Luo, M. Qi and G. J. Cheng, *Science*, 2014, **346**, 1352-1356.
27. R. Fabbro, J. Fournier, P. Ballard, D. Devaux and J. Virmont, *J. Appl. Phys.*, 1990, **68**, 775-784.
28. Bredas, J. L.; Street, G. B., *Acc. Chem. Res.* **1985**, 18, 309-315

FIGURES & CAPTIONS

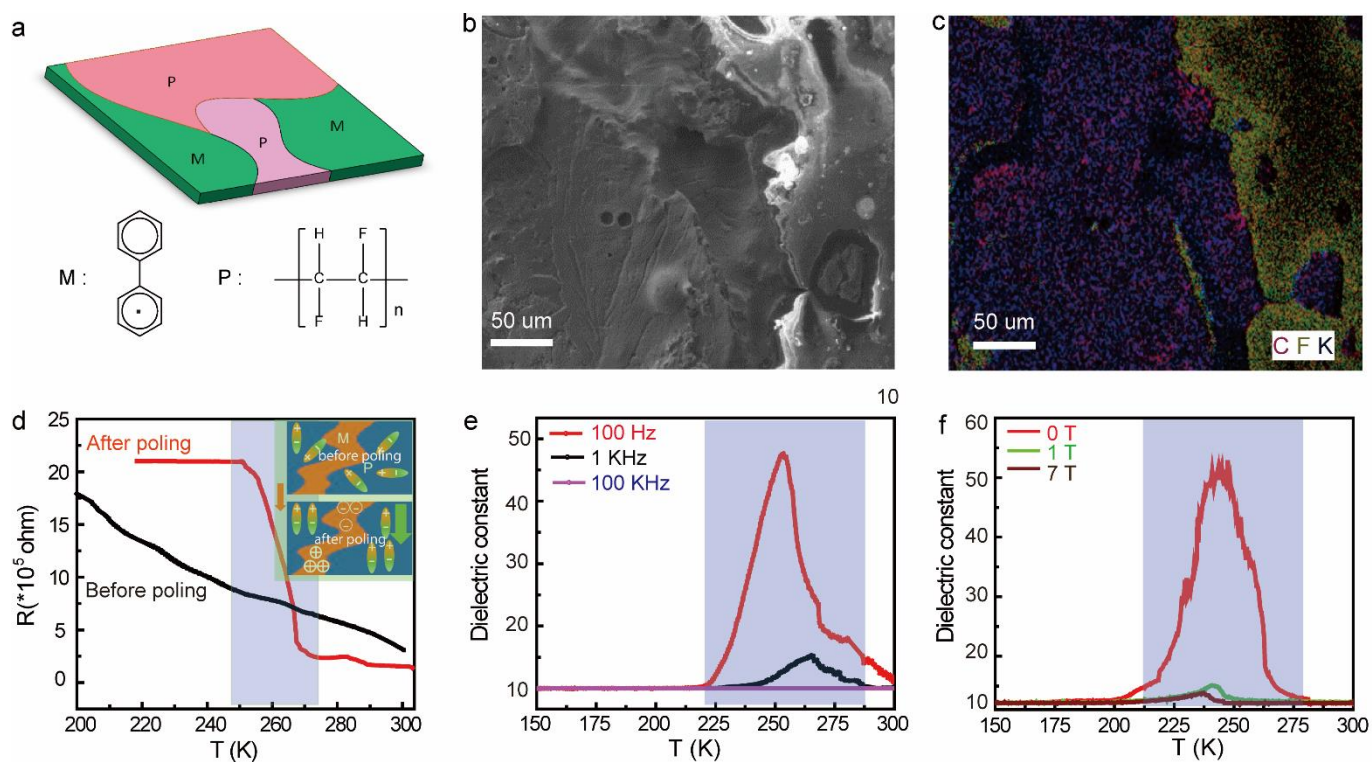


Figure 1. (a) The schematic diagram of the composite sample and the chemical structure of KB radical (M) and PVDF-TrFE (P). (b-c) The SEM image and EDS mapping of KB-PT sample. (d). Temperature dependence of resistance of the KB-PT sample before and after poling with 300 V/cm electrical field. (e) Temperature dependence of relative permittivity of the KB-PT sample at different frequency. (f) Temperature dependence of relative permittivity of the KB-PT sample at different magnetic fields under 1 kHz.

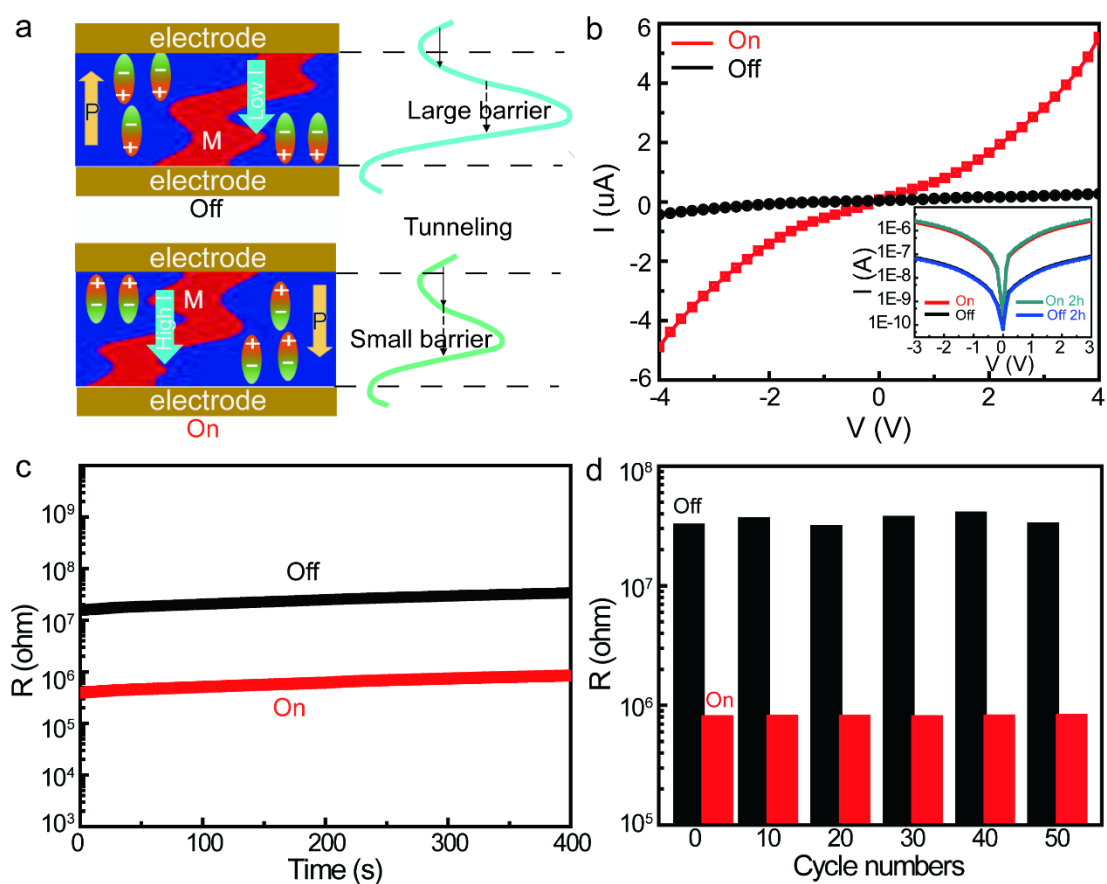


Figure 2. (a) The schematic diagram for the modulation mechanism of the KB-PF samples. (b) The I-V curves of the KB-PF samples in the On and Off states. Inset shows I-V curves for On and Off states at after 2 hours. (c) Retention performance for both On and Off states. (d) Cyclic polarization switching tests the On and Off resistance stability of the KB-PF samples.

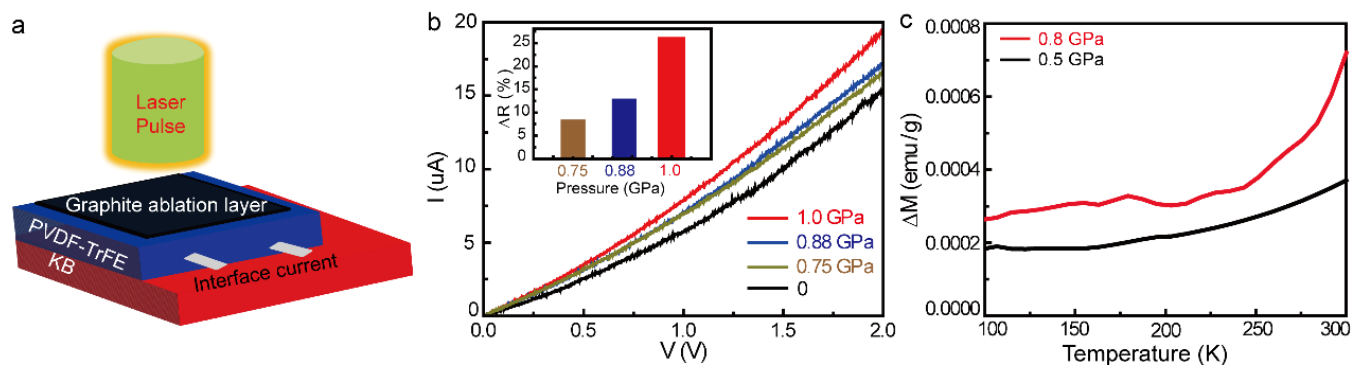


Figure 3. (a) The schematic illustration of laser shock setup. (b) The I-V curves of the KB-PF samples under different pressure induced by laser shock with different intensity. The inset shows the relative resistance change of the KB-PF samples under different pressure induced by laser shock with different intensity. (c) Temperature dependence of magnetization of KB-PF samples under different pressure induced by laser shock with different intensity.

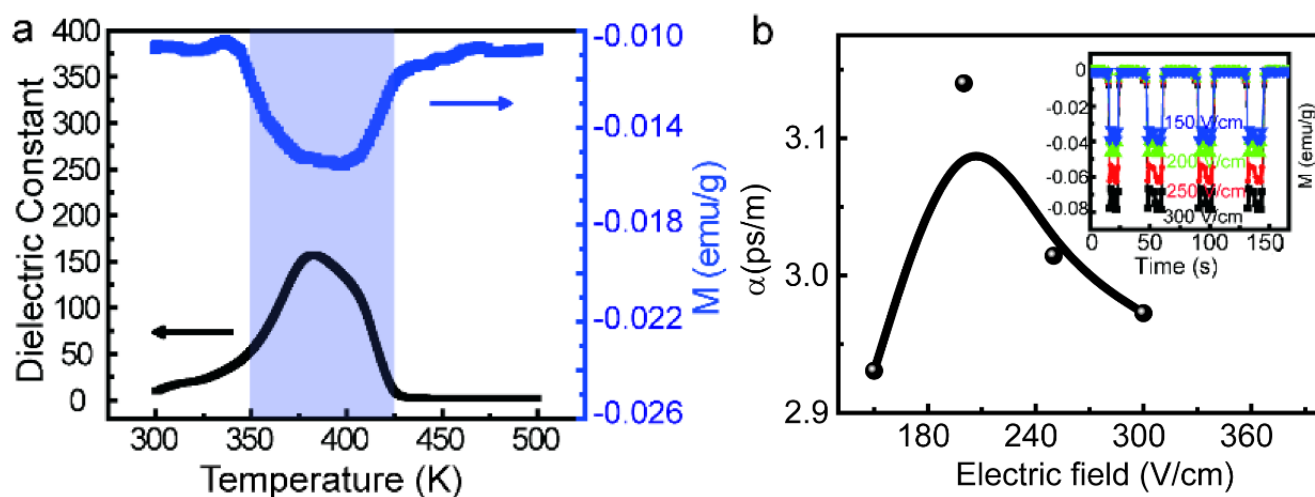


Figure 4. (a) Temperature dependence of magnetization of KB-PF samples and Temperature dependence of relative permittivity of pure PVDF. (b) The converse ME coupling coefficient of KB-PF samples at different electric field. The inset shows the on off switch of magnetization for the KB-PF samples under different electric field.

Table of Contents

